Two-Event Echos in Single-Molecule Kinetics: A Signature of Conformational Fluctuations†

Shilong Yang and Jianshu Cao*

Department of Chemistry, Massachusetts Institute of Technology, Cambridge, Massachusetts 02139

Received: November 30, 2000; In Final Form: March 28, 2001

The relationship between event-averaged measurements and ensemble averaged measurements can be clarified by averaging along single-molecule trajectories. As a result, phenomenological chemical kinetics is shown to contain little information about dynamic disorder, and nonequilibrium relaxation experiments in the bulk state may not be interpreted according to the fluctuation−dissipation relation. The desired information about conformational fluctuations can be inferred from the statistics and correlation of half-reaction events. In particular, the echo time in the two-event probability distribution directly measures the conformational relaxation rate, and the amplitude of the echo probes the variance of the reaction rate. Detailed analysis of four different models (two-channel kinetic scheme, three-channel kinetic scheme, diffusion-modulated reaction, and the Gaussian stochastic rate model) confirms the generality of the two-event echo and its quantitative relations with conformation dynamics. As a general description of the fluctuating rate process, the stochastic rate model and its truncated version provide the flexibility to incorporate various kinetic schemes and functional forms and serve as a first-order model for analyzing single-molecule quantities.

I. Introduction

The issue of multiple time scales is a recurring theme in physical chemistry and has been explored from various perspectives.[1] Traditional chemical kinetics assumes a clear separation of time scales; that is, the rate process in a reactive system occurs on the slowest time scale so that all other motions can be averaged on the reaction time scale to yield dissipation and random noise. Under these assumptions, the depletion from the reactant to the product is a Poisson process and the average population disturbance decays exponentially. However, in proteins and glassy systems, chemical reactions are usually modulated by geometric constraints, slow structural relaxation, and hydrogen bonding and network in aqueous systems. In the presence of such slow environmental fluctuations, the competition between the reaction process and the conformational dynamics leads to nonexponential kinetics and memory effects.[2−8] Yet, such conformational modulation cannot be completely described by phenomenological kinetics and is often not resolved in bulk measurements. In comparison, single-molecule trajectories consist of a chain of correlated reaction events of various durations and thus provide a unique probe to conformational fluctuations. This paper presents quantitative analysis of conformational dynamics as revealed by the two-event echo in single-molecule kinetics.

Advances in optical spectroscopy and microscopy have made it possible to directly measure the optical spectrum along single molecular trajectories and monitor the molecular dynamics and chemical kinetics of individual reactive systems.[9−17] Early experiments pioneered by Moerner and co-workers have investigated the single-molecule emission process in low temperature glasses, which has since been analyzed by Skinner, Silbey, and other groups within the framework of the standard two-level model.[18−22] Recent progress has expanded the regime of single-molecule spectroscopy from low temperatures to room temperatures and from glassy systems to reactive chemical systems and biomolecules. As reviewed by Xie and Trautman,[23] new developments in room temperature single-molecule experiments include observations of spectral fluctuations, translational and rotational diffusion motions, conformational dynamics, fluorescence resonant energy transfer, exciton dynamics, and enzyme reactivity. These new experiments contain rich information that needs theoretical interpretations and models. Of particular relevance are recent studies of nonexponential reaction dynamics in single-molecule kinetics. For example, Hochstrasser coworkers and Rigler co-workers measured the fluorescence decay associated with single DNA and tRNA.[13,14] Geva and Skinner applied a stochastic two-state model to interpret biexponential relaxation in these experiments.[24,25] Xie and co-workers demonstrated slow fluctuations in the turn-over rate of cholesterol oxidation and the dependence of enzymatic turnovers on previous history.[15] This experiment has since inspired several theoretical studies of memory effects in single-molecule kinetics.[26−28] Weiss and co-workers developed fluorescence resonance energy transfer as a means to explore conformational dynamics.[16] Theoretically, a well-studied reactive system is ligand-binding proteins, which exemplify the concept of potential landscapes in protein environments.[3,29,30] Wang and Wolynes explored single-molecule reaction dynamics in fluctuating environments and showed theoretically that the statistics of single reaction events exhibit intermittency and do not follow the Poisson law.[31] Onuchic et al. explored the possibility of using replica correlation functions along single-molecule trajectories to analyze complex energy landscapes.[32] Mukamel and coworkers calculated stochastic trajectories of solvent-controlled electron transfer and demonstrated non-Poisson kinetics in the waiting time distribution function.[33] Metiu and co-workers devised a four-state kinetic scheme to model room-temperature fluorescence of single dye molecules adsorbed on a glass surface.[34] Agmon introduced a diffusion model for the conformational cycle of a single working enzyme.[28] Though much

† Dedicated to Professor Bruce Berne with admiration and affection. Part of the special issue "Bruce Berne Festschrift".

* To whom correspondence should be addressed. E-mail: jianshu@mit.edu.

10.1021/jp004349k CCC: $20.00
Published on Web 05/24/2001

progress has been made, it remains a challenge to quantify dynamic disorder in single-molecule kinetics.

It is well appreciated that single-molecule spectroscopy detects spatial disorder without the usual ensemble averaging in conventional spectroscopy. An equally important advantage of single-molecule techniques is the direct observation of slow variations in reaction kinetics, which are often limited by spectral resolution in conventional bulk experiments. In single-molecule experiments, the traced molecular system interconverts between the dark and bright states so that the observed fluorescence turns on and off intermittently. Such blinking phenomena have been observed in a variety of systems, including low-temperature glasses, quantum dots, molecular aggregates, and biological molecules. The waiting time of each on−off event corresponds to the duration of a single-molecule reaction event, and the statistics of on−off events of various durations record the real-time trajectory of the single reactive system. In a sense, the on−off sequence can be viewed as a *binary code*, which contains the essential information about reaction mechanisms. The key to decipher this code is the statistical analysis of on−off blinking trajectories. The use of single-molecule spectroscopy for detecting dynamic disorder has been demonstrated through the measurements of the fluorescence correlation function, the waiting time distribution function, and the two-event joint distribution function. Though a clear evidence of non-Markovian and non-Poisson kinetics, these single-molecule measurements and related analyses are qualitative and descriptive.

In a recent paper,[27] we have developed theoretical tools to calculate measured single-molecule statistics and have clearly demonstrated the essential difference between ensemble-averaged bulk measurements associated with the population dynamics of full-reactions and event-averaged single-molecule measurements associated with a sequence of half-reactions. In particular, the prediction of the focal time in the single-event distribution function and of the recurrent behavior in the two-event distribution function reveals the nature of conformational landscapes. Similar to the photon echo phenomenon, the recurrence can be understood as the echo signal that is due to the inhomogeneous distribution of environments. Analogous to motion narrowing, in the fast modulation limit, the echo signal vanishes and the single-exponential law is recovered. The height of the echo signal and its position vary with the modulation rate and, hence, can be a sensitive probe of the dynamics disorder resulting from conformational fluctuations.

Because conformational fluctuations are not directly accessible experimentally, dynamic disorder is a *hidden* mechanism that requires quantitative analysis of single-molecule measurements. The prediction of the two-event echo signal in ref 27 holds the promise of characterizing dynamic disorder in single-molecule kinetics. However, questions remain with regards to the generality of the recurrence and the quantitative relationship between the echo and conformational dynamics. This paper will address these questions as follows: General features of modulated reactions are reviewed and examined in section II. Phenomenological kinetics, the fluctuation−dissipation relation, and the detailed balance conditions are formulated and clarified on the basis of event-averaged single-molecule quantities. Then, the two-event echo signal is calculated in section III to section VI respectively for the two-channel model, for the three-channel model, for the diffusion model, and for the Gaussian stochastic model. These calculations show that the distribution and the relaxation rate of conformational fluctuations can be estimated from the echo time and the echo amplitude. Of the four models calculated, the stochastic Gaussian model in section VI provides a general description of rate fluctuations in a similar way as Kubo's stochastic line-shape theory and allows other models to be compared and calibrated.[35,36] We conclude with a summary in section VII.

II. General Considerations of Modulated Reactions

Modulated reaction models have been used for analyzing the fluctuating environment and its effects on chemical kinetics. Early examples include a series of papers by Hynes and coworkers[37,38] on the influence of solvent relaxation on the reaction rate constant and the Agmon−Hopfield model for ligand binding to myoglobin.[3] A recent application is the analysis of Xie's single enzyme turnover experiment.[15,27,28]

A generic modulated reaction model is the *N*-conformational-channel reactive system, illustrated in Figure 1a. A special case of the generic model is the two-channel model system illustrated in Figure 1b of this paper. To be specific, the conformational distribution of the reaction is represented by *N* discretized conformational channels, each associated with a reversible reaction between the dark and bright states, with forward rate $k_{a,i}$ and backward rate $k_{b,i}$. The conformational dynamics is represented by the interconversion rate $\gamma_{a,ij}$ from the *j*th state to the *i*th state when the system is in the bright state *A* (i.e., the on state) and the interconversion rate $\gamma_{b,ij}$ from the *j*th state to the *i*th state when the system is in the dark state *B* (i.e., the off state). The different conformational substates are not directly detectable because only the bright state is monitored by fluorescence emission. In single-molecule experiments, the on/off time measures the duration that a single molecule spends in the bright/dark state, and a trajectory of on−off events records the dynamics of the single reactive system.

The two-channel model in section III and the three-channel model in section IV are examples of the *N*-channel model, the diffusion-modulated reaction in section V is a continuous version of the *N*-channel model, and the stochastic Gaussian model in section VI can be understood as the small variance approximation of the *N*-channel model. In the fast modulation limit, the *N*-channel reaction model reduces to a single-channel reaction with an effective rate constant, whereas in the slow modulation limit, it reduces to an inhomogeneous average of the *N* channels. In the latter limit, the single-molecule system remains ergodic, but the rate variation within a single reaction event can be ignored. We briefly review the *N*-channel reaction model as formulated in section II of ref 27 and then examine general features of the model within the context of single-molecule measurements.

A. Event-Averaged Measurements in Single-Molecule Kinetics. As formulated in ref 27, a reaction process can be decomposed into a forward half-reaction, which turns the bright state to the dark state, and a backward half-reaction, which turns the dark state to the bright state. The master equation for the forward half-reaction of the *N*-conformational substates is written as

$$\dot{\mathbf{P}}_a(t) = -(\mathbf{\Gamma}_a + \mathbf{K}_a)\mathbf{P}_a(t) \tag{1}$$

where the vector $\mathbf{P}_{a,i}$ is the survival probability of being in the *i*th conformational substate, the matrix $\Gamma_{a,ij} = \delta_{ij}\gamma_{a,ii} - \gamma_{a,ij}$, with $\gamma_{a,ii} = \sum_j \gamma_{a,ji}$, describes the conformational kinetics in the bright state, and the matrix $\mathbf{K}_{a,ij} = \delta_{ij}k_{a,i}$ describes the reaction process from the dark state to the bright state. Equation 1 can be formally solved by the Green's function

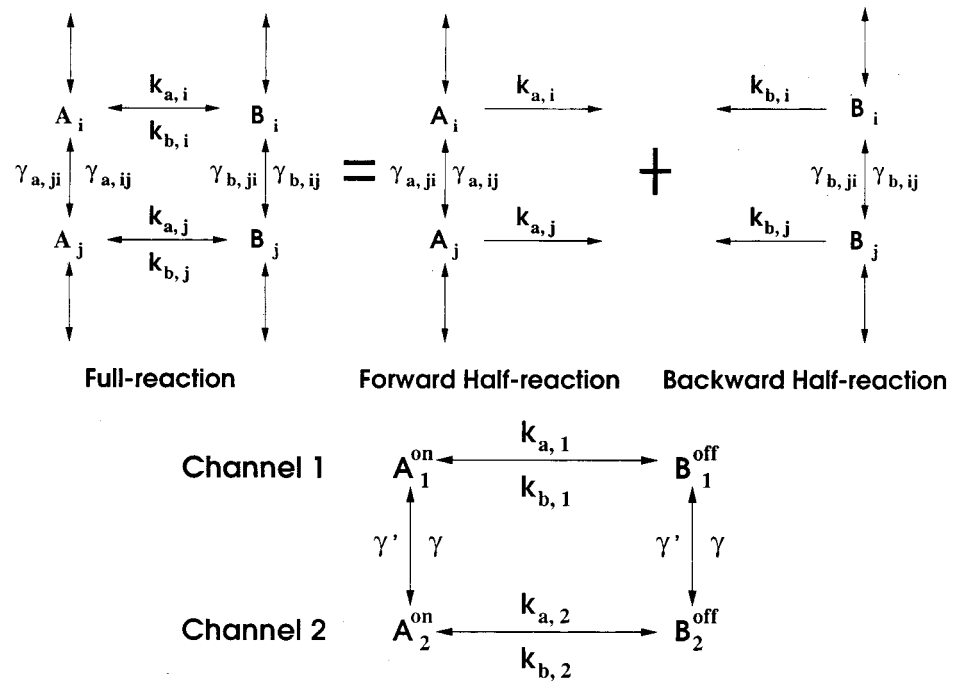

Figure 1. (a) Decomposition of the N conformational-channel reaction model into forward and backward half-reactions. (b) The reaction diagram of the discrete two-channel model. The forward rates are k_{a1} and k_{a2}, the backward rates are k_{b1} and k_{b2}, γ is the conversion rate from channel 1 to channel 2, and γ' is the interconversion rate from channel 2 to channel 1.

$$\mathbf{G}_a(t) = \exp[-t(\mathbf{\Gamma}_a + \mathbf{K}_a)] \tag{2}$$

which is a N-dimensional matrix. The Green's function for the backward half-reaction, $\mathbf{G}_b(t)$, is defined in a similar fashion. The two half-reactions are related through the forward rate constant matrix $\mathbf{K}_a$ and the backward rate constant matrix $\mathbf{K}_b$, yielding the master equation for the full reaction

$$\begin{pmatrix}\dot{\rho}_a(t)\\ \dot{\rho}_b(t)\end{pmatrix} = \begin{pmatrix}-\mathbf{\Gamma}_a - \mathbf{K}_a & \mathbf{K}_b\\ \mathbf{K}_a & -\mathbf{\Gamma}_b - \mathbf{K}_b\end{pmatrix}\begin{pmatrix}\rho_a(t)\\ \rho_b(t)\end{pmatrix} \tag{3}$$

where $[\rho_a(t),\rho_b(t)]$ are the population distribution in the dark and bright states, respectively. The time-independent solution to eq 3 defines the equilibrium distribution

$$(\mathbf{\Gamma}_a + \mathbf{K}_a)\rho_a = \mathbf{K}_b\rho_b \tag{4a}$$

$$(\mathbf{\Gamma}_b + \mathbf{K}_b)\rho_b = \mathbf{K}_a\rho_a \tag{4b}$$

which relate ρ_a to ρ_b and vice versa. It is shown in ref 27 that population evolution measured in bulk experiments is equivalent to the summation of all of the possible reaction events along single-molecule trajectories and the equilibrium ensemble-averaged quantities in the bulk state can be realized by time-averaging single-molecule trajectories over long durations. To explicitly evaluate single-molecule quantities, we introduce the probability density

$$\begin{pmatrix}F_a\\ F_b\end{pmatrix} = N\begin{pmatrix}\mathbf{K}_b\rho_b\\ \mathbf{K}_a\rho_a\end{pmatrix} \tag{5}$$

where F_a is the normalized stationary flux from the bright state to the dark state and F_b is the normalized stationary flux from the dark state to the bright state. It follows from eqs 4a and 4b that $\sum\mathbf{K}_a\rho_a = \sum\mathbf{K}_b\rho_b = N^{-1}$, implying that the total flux is a conserved quantity. Given the stationary fluxes, we can define the distribution function of single on-time events

$$f_a(t) = \sum\mathbf{K}_a\mathbf{G}_a(t)F_a = \sum_{i,j}\mathbf{K}_{a,i}\mathbf{G}_{a,ij}(t)F_{a,j} \tag{6}$$

and the joint distribution function of on−off events

$$f_{ab}(t_2,t_1) = \sum\mathbf{K}_b\mathbf{G}_b(t_2)\mathbf{K}_a\mathbf{G}_a(t_1)F_a \tag{7}$$

which will be evaluated explicitly for several different models in the following sections. These event-averaged quantities cannot be obtained directly in bulk experiments and must be collected along a sequence of reaction events of single reactive systems.

B. Phenomenological Chemical Kinetics. The rate constant used in the phenomenological kinetic description can be interpreted as the average time that the single molecular system spends in a macroscopic state. To be specific, the average on-time is evaluated from the single event distribution function as $\langle t_a\rangle = \int_0^\infty t f_a(t)\,\mathrm{d}t = \sum\mathbf{K}_a(\mathbf{K}_a + \mathbf{\Gamma}_a)^{-2}F_a$, where F_a is the flux from the bright state to the dark state. Using the properties of the equilibrium distribution, $\mathbf{K}_b\rho_b = (\mathbf{K}_a + \Gamma_a)\rho_a$ and $\sum\mathbf{\Gamma}_a = 0$, we have

$$\langle t_a\rangle = \int_0^\infty t f_a(t)\,\mathrm{d}t = \sum(\mathbf{K}_a + \mathbf{\Gamma}_a)\left(\frac{1}{\mathbf{K}_a + \mathbf{\Gamma}_a}\right)^2(\mathbf{K}_a + \mathbf{\Gamma}_a)\rho_a N = \frac{\sum\rho_a}{\sum\mathbf{K}_a\rho_a} \tag{8}$$

The same result can be easily obtained from the average survival time in the bright state, i.e., $\langle t_a\rangle = \int\mathbf{G}_a(t)\,F_a\,\mathrm{d}t$. The average forward rate constant follows as

$$\langle k_a\rangle = \frac{\sum\mathbf{K}_a\rho_a}{\sum\rho_a} \tag{9}$$

which is an inhomogeneous average of forward rate constants and is independent of conformational dynamics. A similar definition can be derived for the backward reaction, $\langle k_b\rangle = \sum\mathbf{K}_b\rho_b/\sum\rho_b$. The ratio of the average forward and backward

reaction rate constants satisfies the phenomenological detailed balance relation

$$\langle k_a \rangle n_a = \langle k_b \rangle n_b \tag{10}$$

where $n_a = \sum \rho_a$ and $n_b = \sum \rho_b$ are respectively the equilibrium populations of the bright state and of the dark state. Consequently, phenomenological chemical kinetics is simply an inhomogeneous average of the microscopic reaction rate constants and therefore does not contain any information about dynamic disorder.

It should be pointed out that relaxation experiments in the bulk state measure the total rate constant $\langle k \rangle = \langle k_a \rangle + \langle k_b \rangle$, and the forward and backward rate constants are obtained through the detailed balance condition in eq 10. In contrast, single-molecule experiments separate the forward and backward half-reactions and uniquely determine the two rate constants. Furthermore, in the context of single molecules, the detailed balance relation in eq 10 is self-evident as long-time averaging along single-molecule trajectories leads to the equilibrium population, which according to eq 8 defines the average rate constant.

High order moments of the on-time distribution function can also be calculated from $\langle t^n \rangle = \int_0^\infty f(t) t^n \, dt$. Generally, higher order moments do not satisfy $\langle t^n \rangle \neq \langle t \rangle^n$, and the decay process is not a Poisson process. Though ensemble-averaged experiments can also measure the waiting-time distribution and high-order moments, such measurements may suffer from spatial disorder and require special initial preparation in order to apply the fluctuation−dissipation theorem (see the next subsection). Even if the waiting-time distribution can be obtained, interpreting memory effects and extracting the modulation rate constant can be difficult. Therefore, single-molecule measurements are more reliable and robust, and the information about dynamic disorder can be inferred from the statistics and correlation of half-reaction events.

C. Fluctuation−Dissipation Relation. A central result of the fluctuation−dissipation theorem is Onsager's regression hypothesis, which relates the relaxation of macroscopic non-equilibrium disturbances to the correlation of spontaneous microscopic fluctuations in an equilibrium system.[39] Application of this theorem to chemical kinetics leads to

$$\frac{\Delta c_a(t)}{\Delta c_a(0)} = \frac{C(t)}{C(0)} = \frac{\mathbf{G}_{aa}(t) - n_a}{1 - n_a} \tag{11}$$

where $\Delta c_a(t) = c_a(t) - c_a(\infty)$ describes the concentration relaxation after a disturbance, measured in ensemble-averaged experiments, and $C(t) = \langle n_a(t) n_a(0) \rangle - n_a^2$ describes the occupation correlation function of the equilibrated reaction system, measured in single-molecule experiments.

We now generalize eq 11 to multichannel reactions. Consider the fluorescent correlation function measured along a single-molecule trajectory, starting from an arbitrary initial time on the trajectory. The probability of starting from a bright state is n_a, and the initial on-time is then averaged over the on-time distribution function, giving

$$\langle n_a(t) n_a(0) \rangle = \frac{\int_0^\infty \mathbf{G}_{aa}(t) \mathbf{G}(t_0) F_a \, dt_0}{\int_0^\infty \mathbf{G}(t_0) F_a \, dt_0} n_a = \sum \mathbf{G}_{aa}(t) \rho_a \tag{12}$$

where the propagation matrix $\mathbf{G}_{aa}(t)$ is the diagonal component of the Green's function solution for the master equation in eq 3. It is shown in ref 27 that $\mathbf{G}_{aa}(t)$ can be expanded in an infinite series of terms in the sequence of single-molecule events

$$\mathbf{G}_{aa}(t) = \mathbf{G}_a(t) + \int_0^t \int_0^{t_1} \mathbf{G}_a(t - t_1) \mathbf{K}_b \mathbf{G}_b(t_1 - t_2) \mathbf{K}_b \mathbf{G}_a(t_2) \, dt_1 \, dt_2 + \ldots \tag{13}$$

where the first term represents staying in the bright state without reaction, the second term represents one sojourn to the dark state, and so on. To measure the macroscopic relaxation, the concentration disturbance $c_a(0)$ in the bright state is introduced according to the equilibrium conformational distribution, i.e.

$$\rho_{a,i}(0) = \frac{\rho_{a,i}}{\sum \rho_{a,i}} c_a(0) \tag{14}$$

Then, the concentration relaxation follows

$$\Delta c_a(t) = \frac{\sum \mathbf{G}_{aa}(t) \rho_{a,t}}{n_a} c_a(0) - n_a c_a(0) \tag{15}$$

where $c_a(\infty) = n_a c(0)$ is the equilibrium concentration of the bright state. Comparing eq 12 and eq 15, we have

$$\frac{\Delta c_a(t)}{\Delta c_a(0)} = \frac{C(t)}{C(0)} = \frac{\sum \mathbf{G}_{aa}(t) \rho_a - n_a^2}{n_a - n_a^2} \tag{16}$$

which is the multichannel version of eq 11. Therefore, the fluctuation−dissipation relation is obeyed under the condition that the initial population disturbance is distributed according to the equilibrium ratio of conformational channels. However, in the relevant scenario discussed in section I, the conformational modulation rate is slower than or comparable to the reaction rate. Then, the initially prepared disturbance will not have enough time to relax in the conformational substates before the concentration starts to decay, thus, violating the initial condition in eq 14 necessary for the fluctuation−dissipation relation in eq 16. Consequently, the initial preparation of relaxation experiments in the bulk state must be taken into consideration in interpreting conformational distribution and dynamics.

Finally, we simplify eq 16 by noting that the asymptotic limit of $\mathbf{G}_{aa}(t)$ is the equilibrium distribution ρ_a. Thus, the propogator $\mathbf{G}_{aa}(t)$ can be decomposed as $\mathbf{G}_{aa}(t) = \rho_a + \mathbf{G}'_{aa}(t)$, which allows us to rewrite the fluorescence correlation function as

$$\frac{C(t)}{C(0)} = \frac{\sum \mathbf{G}'_{aa}(t) \rho_a}{n_a n_b} \tag{17}$$

where $\mathbf{G}'_{aa}$ is the time-dependent part of the Green's function.

D. Detailed Balance Conditions. The conservation of the population flux requires an overall balance relation between the bright state and the dark state, as explicitly given in eq 10. Although this condition conserves the total flux, it does not exclude the possibility of a net current between different conformational channels. To exclude this possibility, the forward flux and backward flux must be equal

$$\mathbf{K}_a \rho_a = \mathbf{K}_b \rho_b \tag{18}$$

which is a more stringent balance relation than eq 10. It follows from eqs 4a and 4b that

$$\mathbf{\Gamma}_a \rho_a = \mathbf{\Gamma}_b \rho_b = 0 \tag{19}$$

which are the detailed balance conditions for the equilibrium conformational distributions in the dark state and the bright state,

respectively. Furthermore, it is reasonable to assume that the conformational dynamics are the same for the bright state and for the dark state, i.e., $\mathbf{\Gamma}_a = \mathbf{\Gamma}_b$. Then, we have $\rho_a \propto \rho_b$ and

$$\mathbf{K}_b \propto \mathbf{K}_a \tag{20}$$

which means that the ratio between the forward reaction rate constant and backward rate constant is the same for all of the conformational channels. Without loss of generality, this paper analyzes on−off events based on symmetric reactions with $\mathbf{K}_a = \mathbf{K}_b$. As is shown in Figure 3 of ref 27, the nature of the two-event distribution function does not change with the backward reaction; therefore, the echo from the on−off correlation for symmetric reactions is similar to the echo from the on-on correlation for asymmetric reactions.

III. Two-Channel Model

The two-channel model, the simplest scheme of multichannel reactions, has been used to analyze event-averaged quantities and to show that the two-event echo has a strong dependence on the conformational distribution and dynamics.[27] The following derivation generalizes the results in Sec. 3 of ref 27 in that the downward rate γ and the upward rate γ' are different. The master equation for the forward half-reaction is given in eq 1 with $\mathbf{P}_a$, $\mathbf{K}_a$, and $\mathbf{\Gamma}$ defined as

$$\mathbf{P}_a(t) = \begin{pmatrix} P_{a1}(t) \\ P_{a2}(t) \end{pmatrix}, \quad \mathbf{K}_a = \begin{pmatrix} k_{a1} & 0 \\ 0 & k_{a2} \end{pmatrix},$$
$$\mathbf{\Gamma} = \mathbf{\Gamma}_a = \mathbf{\Gamma}_b = \begin{pmatrix} \gamma & -\gamma' \\ -\gamma & \gamma' \end{pmatrix} \tag{21}$$

The Green's function is given by

$$\mathbf{G}_a(t) = \mathrm{e}^{-(\mathbf{K}_a+\mathbf{\Gamma})t} = \frac{1}{\Delta_a}\begin{pmatrix} \Delta_a F_a(t) + (k_{ad}+\gamma_d)E_a(t) & \gamma' E_a(t) \\ \gamma E_a(t) & \Delta_a F_a(t) - (k_{ad}+\gamma_d)E_a(t) \end{pmatrix} \tag{22}$$

where $\Delta_a = \sqrt{\gamma_s^2 + k_{ad}^2 + 2k_{ad}\gamma_d}$, $k_{ad} = (k_{a2} - k_{a1})/2$, $k_{as} = (k_{a2} + k_{a1})2$, $\gamma_s = (\gamma + \gamma')/2$, $\gamma_d = (\gamma' - \gamma)/2$, $z_{a\pm} = k_{as} + \gamma_s \pm \Delta_a$, $F_a(t) = (\mathrm{e}^{-z_{a-}t} + \mathrm{e}^{-z_{a+}t})/2$, and $E_a(t) = (\mathrm{e}^{-z_{a-}t} - \mathrm{e}^{-z_{a+}t})/2$. These expressions reduce to eq 14 in ref 27 when $\gamma = \gamma'$. The backward Green's function can be obtained in the same fashion. The master equation of the full reaction, given in eq 3, has a stationary solution

$$\begin{pmatrix} \rho_{a1} \\ \rho_{a2} \\ \rho_{b1} \\ \rho_{b2} \end{pmatrix} = C \begin{pmatrix} \gamma'[\gamma k_{b2} + \gamma' k_{b1} + k_{b1}(k_{a2} + k_{b2})] \\ \gamma[\gamma k_{b2} + \gamma' k_{b1} + k_{b2}(k_{a1} + k_{b1})] \\ \gamma'[\gamma k_{a2} + \gamma' k_{a1} + k_{a1}(k_{a2} + k_{b2})] \\ \gamma[\gamma k_{a2} + \gamma' k_{a1} + k_{a2}(k_{a1} + k_{b1})] \end{pmatrix} \tag{23}$$

where $C^{-1} = (\gamma + \gamma')[\gamma(k_{a2} + k_{b2}) + \gamma'(k_{a1} + k_{b1}) + (k_{a1} + k_{b1})(k_{a2} + k_{b2})]$. The equilibrium flux from the bright state to the dark state is $F_b = N\mathbf{K}_a\rho_a$, and that from the dark state to the bright state is $F_a = N\mathbf{K}_b\rho_b$. The normalization factor is $N^{-1} = \sum\mathbf{K}_b\rho_b = \sum\mathbf{K}_a\rho_a = \gamma^2 k_{a2}k_{b2} + \gamma'^2 k_{a1}k_{b1} + \gamma\gamma'(k_{a2}k_{b1} + k_{a1}k_{b2}) + \gamma(k_{a1} + k_{b1})k_{a2}k_{b2} + \gamma'(k_{a2} + k_{b2})k_{a1}k_{b1}$. Thus, the distribution function of on-time events is

$$f_a(t) = \sum\mathbf{K}_a\mathbf{G}_a(t)F_a = \frac{\langle\mathbf{K}_a\mathrm{e}^{-(\mathbf{K}_a+\mathbf{\Gamma})t}\mathbf{K}_b\rangle}{\langle\mathbf{K}_b\rangle} \tag{24}$$

where $\langle\cdots\rangle$ denotes an average over the equilibrium population distribution in the dark state. The distribution function of off-time events is defined in the same fashion. The joint distribution function of on−off events is defined as

$$f_{ab}(t_1,t_2) = \sum\mathbf{K}_b\mathbf{G}_b(t_2)\mathbf{K}_a\mathbf{G}_a(t_1)F_a = \frac{\langle\mathbf{K}_b\mathrm{e}^{-(\mathbf{K}_b+\mathbf{\Gamma})t_2}\mathbf{K}_a\mathrm{e}^{-(\mathbf{K}_a+\mathbf{\Gamma})t_1}\mathbf{K}_b\rangle}{\langle\mathbf{K}_b\rangle} \tag{25}$$

which can be used to analyze memory effects. In particular, the difference function $\delta(t_1,t_2) = f_{ab}(t_1,t_2) - f_a(t_1)f_b(t_2)$ is given explicitly as

$$\delta(t_1,t_2) = \delta(0)\frac{[\Delta_a F_a(t_1) - (k_{a,s}+\gamma_s)E_a(t_1)][\Delta_b F_b(t_2) - (k_{b,s}+\gamma_s)E_b(t_2)]}{\Delta_a\Delta_b} \tag{26}$$

where the initial value $\delta(0)$ is a complicated function of the reaction rate constants and the interconversion rates.

For simplicity, we consider symmetric reactions with $\mathbf{K}_a = \mathbf{K}_b = \mathbf{K}$. In this case, the forward and backward propagators become the same

$$\mathbf{G}(t) = \mathrm{e}^{-(\mathbf{K}+\mathbf{\Gamma})t}\frac{1}{\Delta}\begin{pmatrix} \Delta F(t) + (k_d+\gamma_d)E(t) & \gamma' E(t) \\ \gamma E(t) & \Delta F(t) - (k_d+\gamma_d)E(t) \end{pmatrix} \tag{27}$$

where $\Delta_a = \Delta_b = \Delta$, $E_a(t) = E_b(t) = E(t)$, and $F_a(t) = F_b(t) = F(t)$. The equilibrium populations are $\rho_{a1} = \rho_{b1} = \gamma'/[2(\gamma + \gamma')]$ and $\rho_{a2} = \rho_{b2} = \gamma/[2(\gamma + \gamma')]$, which depend only on the interconversion rates. The difference function $\delta(t_1,t_2)$ is simplified to

$$\delta(t_1,t_2) = \delta(0)\frac{[\Delta F(t_1) - (k_s+\gamma_s)E(t_1)][\Delta F(t_2) - (k_s+\gamma_s)E(t_2)]}{\Delta^2} \tag{28}$$

where the initial value is

$$\delta(0) = \frac{k_d^2(k_s^2 - k_d^2)(\gamma_s^2 - \gamma_d^2)}{(k_d\gamma_d - k_s\gamma_s)^2} \tag{29}$$

with $k_d = (k_2 - k_1)/2$ and $k_s = (k_2 + k_1)/2$. The same-time difference function follows eq 28 as $\delta(t) = \delta(t,t)$. From $\mathrm{d}\delta(t)/\mathrm{d}t = 0$, the focal time of the same-time difference function is found as

$$t_\mathrm{f} = \frac{1}{2\Delta}\ln\frac{z_+}{z_-} = \frac{1}{2\Delta}\ln\frac{k_s+\gamma_s+\Delta}{k_s+\gamma_s-\Delta} \tag{30}$$

where the difference function is zero, $\delta(t_\mathrm{f}) = 0$, and the echo time is found to be related to the focal time via

$$t_\mathrm{e} = 2t_\mathrm{f} \tag{31}$$

where the amplitude of the echo is

$$\delta(t_\mathrm{e}) = \delta(0)\left(\frac{\eta-1}{\eta+1}\right)^{2\eta} \tag{32}$$

with $\eta = (k_s + \gamma_s)/\Delta$. From eq 28, we find a minimum along the t_1 axis or the t_2 axis at the echo time, respectively.

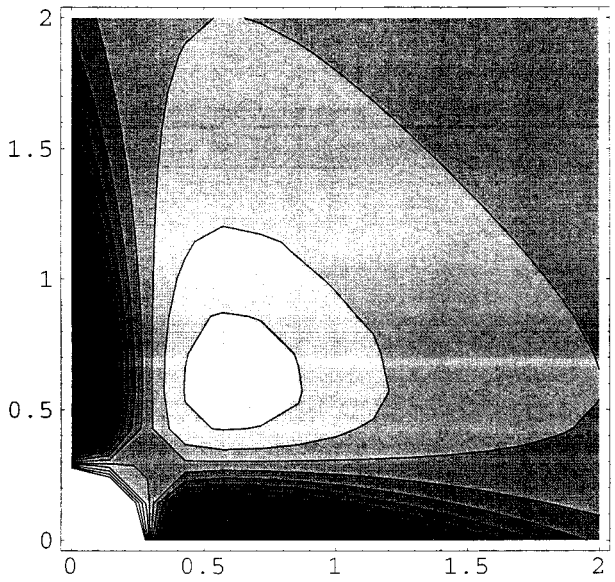

Figure 2. Two-dimensional contour plot of the joint distribution function of two events $f(t_1,t_2) - f(t_1)f(t_2)$ for the two-channel model with $k_1 = 2$, $k_2 = 4$, and $\gamma = \gamma' = 0.5$. At $t = t_e$, $\delta(t_1,t_2)$ reaches its maximum along the diagonal and its minimum along each time axis.

TABLE 1: Echo Time in the Two-Channel Model with $k_1 = 2.5$ and $k_2 = 3.5$[a]

γ	0	0.5	1.0	1.5	2.0	2.5
$t_{e,pred}$	0.667	0.571	0.500	0.444	0.400	0.364
$t_{e,meas}$	0.645	0.555	0.485	0.440	0.390	0.375
error	3.4%	2.9%	3.1%	0.9%	2.6%	3.7%

[a] $t_{e,pred}$ is evaluated from $t_{e,pred} = 2/(\langle k\rangle + \gamma)$, and $t_{e,meas}$ is obtained from the numerical calculation of $\delta(t)$. $\gamma = \gamma'$ is the interconversion rate. The error is defined as $|t_{e,pred} - t_{e,meas}|/t_{e,meas} \times 100\%$.

The same-time difference function $\delta(t)$ is a complicated function of reaction rate constants and conformational interconversion rates. To facilitate our analysis, we consider several special cases.

1. Figure 2 is a two-dimensional contour plot of the difference distribution function, $\delta(t_1,t_2)$, for $k_1 = 2$, $k_2 = 4$, and $\gamma = \gamma' = 0.5$. As predicted by eq 28, the contour clearly shows a minimum at $t_f = 0.287$ and a maximum at $t_e = 0.575$ along the diagonal axis, as well as a minimum at the focal time t_e along the t_1 and t_2 axis.

2. When the reactive time scale is relatively fast, i.e., $k_d,\gamma \ll k_s$, we have

$$t_e = \frac{1}{\Delta}\ln\left[\frac{k_s + \gamma_s + \Delta}{k_s + \gamma_s - \Delta}\right] \approx \frac{2}{k_s + \gamma_s} \tag{33}$$

where the approximate relation directly measures the average modulation rate for a given rate constant. In Table 1, for $k_s = 3.0$ and $k_d = 0.5$, the echo time predicted from eq 33, $t_{e,pred}$, is compared with the echo time measured from the same-time distribution function, $t_{e,meas}$. For a wide range of modulation rates, these two sets of echo times agree within an error less than 10%.

3. Equation 32 gives the amplitude of the echo, which, under the condition of $k_d < \gamma < k_s$, can be shown to be proportional to the variance k_d^2, i.e.

$$\delta(t_e) \propto k_d^{\,2} \tag{34}$$

In Figure 3, the same-time difference distribution function $\delta(t)$ is plotted for $k_s = 2.5$ and $\gamma = \gamma' = 2.0$. As seen from the plot,

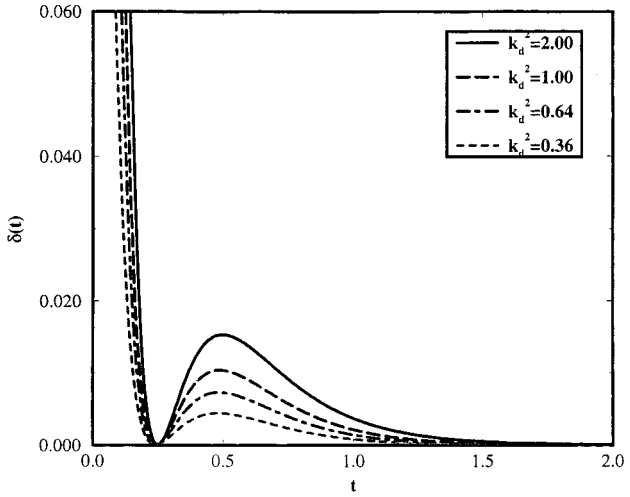

Figure 3. Same-time difference function in the two-channel model where $\gamma = \gamma' = 2.0$ and $k_s = 2.5$. The echo time predicted by $t_e = 2t_f \approx 2/(\langle k\rangle + \gamma)$ is confirmed with small error at large k_d where $k_d \ll k_s$ is not strictly followed. The amplitude of the echo is approximately proportional to the variance in the rate constant.

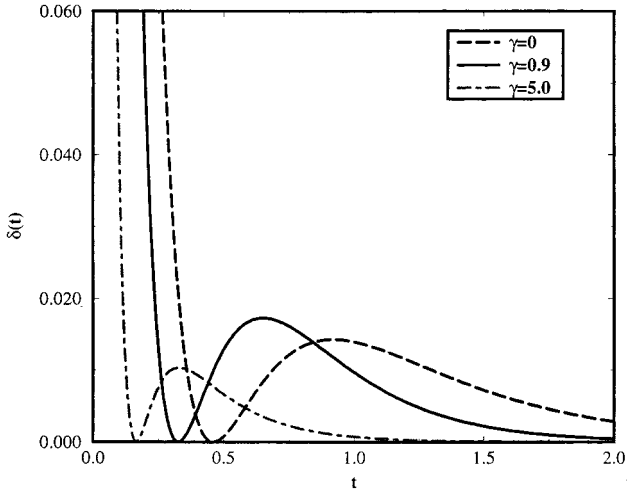

Figure 4. Same-time difference function in the two-channel model when $\gamma = \gamma'$, $k_1 = 1$, and $k_2 = 4$. The maximal echo is reached when $\gamma = k_d^2/k_s$. As predicted by $t_e = 2t_f \approx 2/(\langle k\rangle) + \gamma)$, the echo time decreases as the modulation rate γ increases.

the echo amplitude increases proportionally with k_d^2, even for relatively large k_d^2. The plot also confirms that the focal time is half the echo time and that both times are invariant to k_d^2.

4. In the case of equal interconversion rates, $\gamma' = \gamma$, eq 32 still applies with $\delta(0) = k_d^2(k_s^2 - k_d^2)/k_s^2$ and $\eta = (k_s + \gamma)/\sqrt{k_d^{\,2}+\gamma^2}$. It can be shown that the amplitude of the echo $\delta(t_e)$ reaches its maximum at $\eta_{max} = \sqrt{k_s^{\,2}+k_d^{\,2}}/k_d$ when

$$\gamma = \frac{k_d^{\,2}}{k_s} = \frac{\langle(\delta k)^2\rangle}{\langle k\rangle} \tag{35}$$

which is the critical conformational interconversion rate for the maximal echo. Figure 4 is a plot of the same-time difference distribution function for $k_1 = 1$, $k_2 = 4$, and several values of γ. The maximal echo occurs at $\gamma = 0.9$, which follows the critical condition in eq 35. It can also be noticed in Figure 4 that the focal time and the echo time decrease as γ increases, as predicted by eq 33.

5. In the slow modulation limit, $\gamma,\gamma' \ll k_{1,2}$, which is a possible scenario for sluggish environments, eq 28 is simplified to

$$\delta(t_e) = \frac{(k_2 - k_1)^2}{4} \frac{R_k R_\gamma}{(R_k + R_\gamma)^2} \left(\frac{R_k - 1}{R_k + 1}\right)^{2R_k} \tag{36}$$

where $R_k = k_2/k_1$ and $R_\gamma = \gamma'/\gamma$. With k_1 and k_2 fixed, the maximal echo occurs at

$$R_\gamma = R_k \quad \text{or} \quad \frac{k_2}{k_1} = \frac{\gamma'}{\gamma} = \frac{\rho_1}{\rho_2} \tag{37}$$

which implies a detailed balance relationship between the two channels, $k_1\rho_1 = k_2\rho_2$. As shown in Figure 5, in the slow modulation limit, t_f and t_e are fixed at $\ln[k_2/k_1]/(k_2 - k_1)$ and 2 $\ln[k_2/k_1]/(k_2 - k_1)$, respectively. The maximal echo is achieved when the ratio in eq 37 is satisfied at $R_\gamma = 4$. It can be argued from this example that memory effects of conformational modulation can be measured by the variation of the reaction rate constants $\langle(\delta k)^2\rangle$ and the variance of the flux $\langle(\delta k\rho)^2\rangle$. To have the maximal echo, $\langle(\delta k)^2\rangle$ should be maximized, whereas $\langle(\delta k\rho)^2\rangle$ should be minimized.

IV. Three-Channel Model

To explore the generality of the recurrent behavior of the two-event distribution function, we study a cyclic three-channel model with

$$\mathbf{\Gamma} = \begin{pmatrix} 2\gamma & -\gamma & -\gamma \\ -\gamma & 2\gamma & \gamma \\ -\gamma & -\gamma & 2\gamma \end{pmatrix}; \quad \mathbf{K}_a = \mathbf{K}_b = \begin{pmatrix} k_1 & 0 & 0 \\ 0 & k_2 & 0 \\ 0 & 0 & k_3 \end{pmatrix} \tag{38}$$

Numerical calculations clearly demonstrate the basic features consistent with our observations in the two-channel model:

1. Figure 6 is a contour of the difference function $\delta(t_1,t_2)$ calculated for the three-channel model with the modulation rate $\gamma = 0.5$ and the three reaction rates $k_1 = 2.5$, $k_2 = 3.0$, and $k_3 = 3.5$, respectively. As seen from the two-dimensional contour, the diagonal distribution has a minimum at the focal time t_f and a maximum at the echo time $t_e = 2t_f$, whereas both $\delta(t,0)$ and $\delta(0,t)$ have a minimum at the echo time t_e.

2. In Table 2, $t_{e,pred}$ calculated from $t_e \approx 2/(\langle k\rangle + \gamma)$ agrees well with $t_{e,meas}$ measured by numerical calculations, for the three-channel model with $k_1 = 2.5$, $k_2 = 3.0$, and $k_3 = 3.5$. The error is within 10% over a range of γ.

3. Figure 7 shows the linear dependence of the amplitude of the two-event echo on $\langle(\delta k)^2\rangle$ for the three-channel model described earlier. Again, the echo time and the focal time are invariant to $\langle(\delta k)^2\rangle$ and follow the estimation $t_e = 2/(\langle k\rangle + \gamma)$.

4. Figure 8 shows the same-time difference function for several values of γ. As predicted, the maximal echo occurs at $\gamma \approx k_d^2/\langle k\rangle$ and the focal time is half the echo time and decreases as γ increases.

We also calculated other three-channel and four-channel models with various parameters and geometries and found essentially the same behavior. Thus, we believe that these features are universal for discretized multiple-channel models. In the next section, we will investigate the diffusion reaction model.

V. Diffusion Model

The diffusion-modulated reaction was first introduced by Agmon and Hopfield to describe the ligand binding in myoglobin, and was analyzed by Zwanzig and elaborated by Wang and Wolynes[3,29,31,40] Similar models have been applied for studying solvent-controlled electron transfer.[41−45] The diffusion reaction model describes a reactive system modulated by a diffusive coordinate, which represents collective environmental motions. The diffusion coordinate is described by the Smoluchowski operator

$$\hat{L}_D = \lambda\theta \frac{\partial}{\partial x}\left(\frac{\partial}{\partial x} + \frac{x}{\theta}\right) \tag{39}$$

where λ characterizes the relaxation time scale of the diffusive

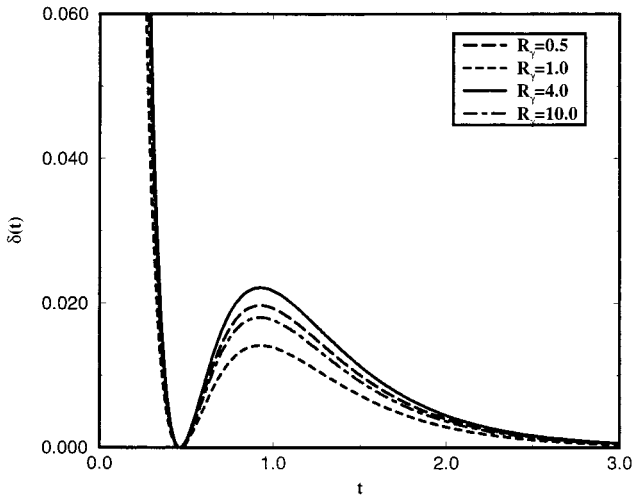

Figure 5. Conformational conversion rate dependence of the two-event echo in the two-channel model with $k_1 = 1$ and $k_2 = 4$. In this slow modulation limit, γ and γ' are the downward and upward interconversion rates, respectively, and $\gamma,\gamma' \ll k_{1,2}$. R_γ is the ratio of the two interconversion rates, $R_\gamma = \gamma'/\gamma$.

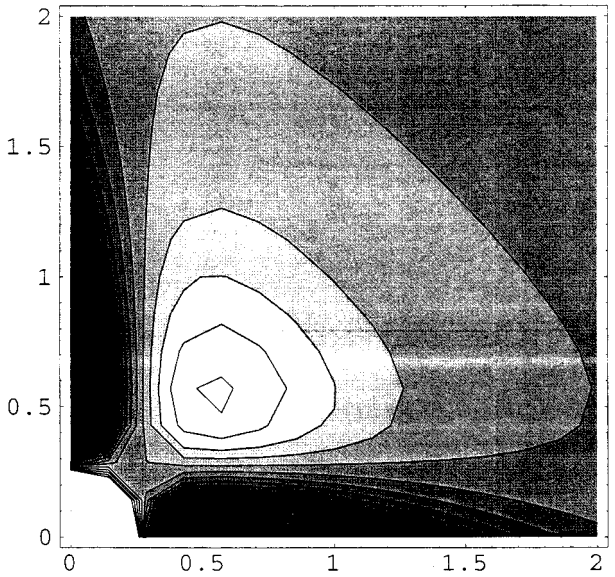

Figure 6. Two-dimensional contour plot of $\delta(t_1,t_2)$ for the three-channel model with $k_1 = 2.5$, $k_2 = 3$, $k_3 = 3.5$, and $\gamma = \gamma' = 0.5$. It is clearly shown that $t_e \doteq 2t_f \approx 2/(\langle k\rangle + \gamma)$ and that both $\delta(0,t)$ and $\delta(t,0)$ reach their minima at $t = t_e$.

TABLE 2: Echo Time in the Three-Channel Model with k_1, k_2, and k_3 as 2.5, 3.0, and 3.5, Respectively[a]

γ	0	0.5	1.0	1.5	2.0	2.5
$t_{e,pred}$	0.667	0.571	0.500	0.444	0.400	0.364
$t_{e,meas}$	0.665	0.550	0.465	0.410	0.370	0.335
error	0.3%	3.8%	7.5%	8.3%	8.1%	8.7%

[a] $t_{e,pred}$ is evaluated from $t_{e,pred} = 2/(\langle k\rangle + \gamma)$, and $t_{e,meas}$ is obtained from the numerical calculation of $\delta(t)$. The error is defined as $|t_{e,pred} - t_{e,meas}|/t_{e,meas} \times 100\%$.

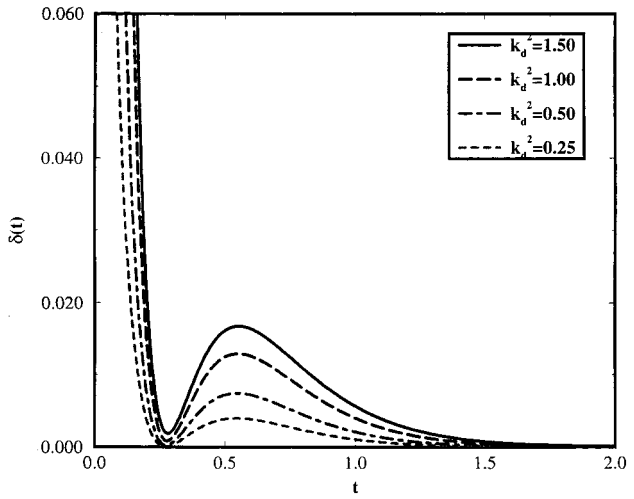

Figure 7. Same-time difference function $\delta(t)$ in the three-channel model with $\langle k\rangle = 3.0$ and $\gamma = 0.5$. It is clearly shown that the two-event echo increases as k_d^2 increases.

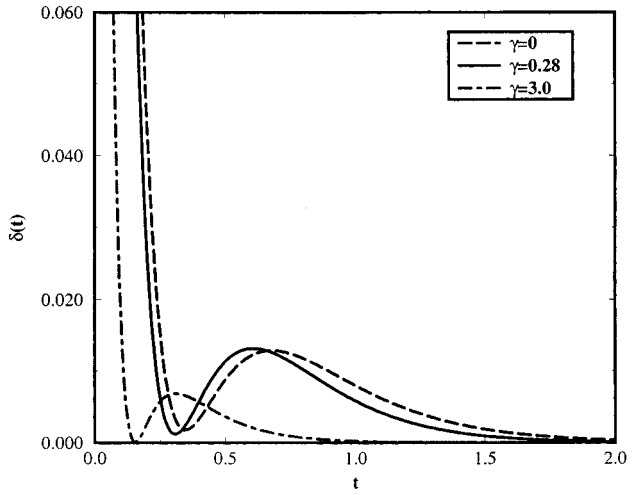

Figure 8. Same-time difference function $\delta(t)$ in the three-channel model with $\langle k\rangle = 3.0$ and $k_d^2 = 1.0$. It is clearly shown that the echo time decreases as γ increases. The maximum echo occurs at $\gamma \approx k_d^2/\langle k\rangle \approx 0.3$, as predicted in eq 35.

solvent, θ is the variance of the equilibrium distribution of the diffusion coordinate, and $\lambda\theta = D$ is the diffusion constant. The relaxation rate λ in the diffusion model is equivalent to the interconversion rate γ in the two-channel model. The reaction rate $k(x)$ is related to the diffusion coordinate x by $k(x) = \kappa x^2$, with κ the proportionality coefficient, so that the survival probability satisfies

$$\frac{\partial}{\partial t}P(x,t) = -k(x)\,P(x,t) + \hat{L}_{\mathrm{D}}P(x,t) \tag{40}$$

The corresponding Green's function is derived in Appendix A, giving

$$G(x,y,t) = \mathrm{e}^{-\lambda(s-1)t/2}\left[\frac{s}{2\pi\theta(1-\mathrm{e}^{-2\lambda st})}\right]^{1/2} \exp\left[-\frac{s(x-y\mathrm{e}^{-\lambda st})^2}{2\theta(1-\mathrm{e}^{-2\lambda st})} + \frac{(s-1)(x^2-y^2)}{4\theta}\right] \tag{41}$$

where $s = \sqrt{1+4\kappa\theta/\lambda}$ represents the coupling of the two time scales associated with diffusion and rate processes. The equilibrium population obtained from $\hat{L}_{\mathrm{D}}\rho_{\mathrm{eq}}(x) = 0$ is a Gaussian function, $\rho_{\mathrm{eq}}(x) = \mathrm{e}^{-x^2/(2\theta)}/\sqrt{2\pi\theta}$; hence, we have $\langle k\rangle = \kappa\theta$ and $\langle(\delta k)^2\rangle = 2\kappa^2\theta^2$.

To study the master equation for the full rection, we consider the symmetric case, where the bright and dark states, labeled as a and b, respectively, have the same relative rate:

$$\begin{pmatrix}\dot{\rho}_a(x,t)\\ \dot{\rho}_b(x,t)\end{pmatrix} = \begin{pmatrix}-k(x) - \hat{L}_{\mathrm{D}} & k(x)\\ k(x) & -k(x) - \hat{L}_{\mathrm{D}}\end{pmatrix}\begin{pmatrix}\rho_a(x,t)\\ \rho_b(x,t)\end{pmatrix} \tag{42}$$

With the Green's function in eq 41, we obtain the distribution function of on-time events

$$f(t) = \frac{\langle\int_{-\infty}^{\infty}\int_{-\infty}^{\infty}\mathrm{d}x\,\mathrm{d}y\,k(x)G(x,y,t)k(y)\rangle}{\langle k(y)\rangle} = \frac{\sqrt{s}\kappa\theta[2s^2+\varphi(t)^2]}{[\varphi(t/2)\psi(t/2)]^{5/2}}\exp\left[\frac{\lambda t}{2}\right] \tag{43}$$

and the joint distribution function of on−off events

$$f(t,t) = \frac{\langle\int_{-\infty}^{\infty}\int_{-\infty}^{\infty}\int_{-\infty}^{\infty}\mathrm{d}x\,\mathrm{d}y\,\mathrm{d}z\,k(x)G(x,y,t)k(y)G(y,z,t)k(z)\rangle}{\langle k(z)\rangle} = \frac{\kappa^2\theta^2[(\varphi(2t)+2s)^2+6s^2]}{\sqrt{s}\varphi(t)^{3/2}\psi(t)^{7/2}}\exp[\lambda t] \tag{44}$$

where $\varphi(t) = [(s+1)\mathrm{e}^{\lambda st} + (s-1)\mathrm{e}^{-\lambda st}]/2$ and $\psi(t) = [(s+1)\mathrm{e}^{\lambda st} - (s-1)\mathrm{e}^{-\lambda st}]/2$. The same-time difference function $\delta(t) = f(t,t) - f(t)^2$ is given by

$$\delta(t) = \kappa^2\theta^2\left[\frac{(\varphi(2t)+2s)^2+6s^2}{\sqrt{s}\varphi(t)^{3/2}\psi(t)^{7/2}} - \frac{s(\varphi(t)^2+2s^2)^2}{\varphi(t/2)^5\psi(t/2)^5}\right]\exp[\lambda t] \tag{45}$$

with the initial value $\delta(0) = 6\kappa^2\theta^2$.

These single-molecule quantities are complicated functions of $\kappa\theta/\lambda$. We examine their behavior in several limiting cases.

1. In the fast modulation limit, $\lambda \to \infty$, the distribution functions become

$$f(t) \to \kappa\theta\exp[-\kappa\theta t] \tag{46a}$$

$$f(t,t) \to \kappa^2\theta^2\exp[-2\kappa\theta t] \tag{46b}$$

$$\delta(t) \approx 0 \tag{46c}$$

thus resulting in single-exponential kinetics with an effective rate constant $k_{eff} = \kappa\theta$.

2. In the slow modulation limit, $\lambda \to 0$, the Green's function simplifies to

$$G(x,y,t) = \delta(x-y)\exp[-\kappa x^2 t] \tag{47}$$

Then, the event averaged distribution functions decay by power law

$$f(t) \to \frac{3\kappa\theta}{(1+2\kappa\theta t)^{5/2}} \tag{48a}$$

$$f(t,t) \to \frac{15\kappa^2\theta^2}{(1+4\kappa\theta t)^{7/2}} \tag{48b}$$

$$\delta(t) \approx 15\kappa^2\theta^2/(1+4\kappa\theta t)^{7/2} - 9\kappa^2\theta^2/(1+2\kappa\theta t)^5 \tag{48c}$$

which are a result of inhomogeneous averaging of the rate distribution. Because the flux $k(x)\rho_{\mathrm{eq}}(x)$ is distributed around x

$= 0$, the diffusion model in the slow modulation limit effectively reduces to a single channel, and therefore, no echo is observed in this limit. However, if a sufficiently large bias is introduced into the rate constant, $k(x) = \kappa(x - x_b)^2$, the diffusion model maps to a two-channel model and the echo can be observed in the inhomogeneous limit.

3. In the long time regime, $f(t)$ and $f(t,t)$, both decay exponentially as

$$f(t) \rightarrow \frac{8\sqrt{s}\kappa\theta}{(s+1)^3}\exp\left[-\frac{\lambda}{2}(s-1)t\right] \tag{49a}$$

$$f(t,t) \rightarrow \frac{8\kappa^2\theta^2}{\sqrt{s}(s+1)^3}\exp[-\lambda(s-1)t] \tag{49b}$$

$$\delta(t) \propto \exp[-\lambda(s-1)t] \tag{49c}$$

with the effective rate constant $k_{\text{eff}} = \lambda(s-1)/2$.

4. In the short time regime, we expand the distribution functions to first order in t

$$f(t) \rightarrow 3\kappa\theta\left(1 - \frac{4}{3}\lambda t - 5\kappa\theta t + O[t^2]\right) \tag{50a}$$

$$f(t,t) \rightarrow 15\kappa^2\theta^2\left(1 - \frac{16}{5}\lambda t - 14\kappa\theta t + O[t^2]\right) \tag{50b}$$

$$\delta(t) \approx 6\kappa^2\theta^2\left(1 - \frac{20}{3}\lambda t - 30\kappa\theta t + O[t^2]\right) \tag{50c}$$

which predict the initial decay because of the reaction and diffusion processes.

To facilitate calculations, we use $1/\kappa\theta$ as the unit time and normalize function $\delta(t)$ by $\delta(0)$. Thus, the reduced same-time difference function reads

$$\tilde{\delta}(\tilde{t}) = \frac{\delta(t)}{\delta(0)} = \frac{e^{4\tilde{t}/(s^2-1)}}{6}\left[\frac{(\tilde{\varphi}(2\tilde{t}) + 2s)^2 + 6s^2}{\sqrt{s}\tilde{\varphi}(\tilde{t})^{3/2}\tilde{\psi}(\tilde{t})^{7/2}} - \frac{s(\tilde{\varphi}(\tilde{t})^2 + 2s^2)^2}{\tilde{\varphi}(\tilde{t}/2)^5\tilde{\psi}(\tilde{t}/2)^5}\right] \tag{51}$$

where $\tilde{t} = t\kappa\theta$, $\tilde{\varphi}(\tilde{j}) = [(s+1)e^{4s\tilde{t}/(s^2-1)} + (s-1)e^{-4s\tilde{t}/(s^2-1)}]/2$ and $\tilde{\psi}(\tilde{t}) = [(s+1)e^{4s\tilde{t}/(s^2-1)} - (s-1)e^{-4s\tilde{t}/(s^2-1)}]/2$. As shown in Figure 9, the same-time distribution function $\tilde{\delta}(\tilde{t})$ has an echo in the region $1 < s < 2.81$ and reaches its maximum amplitude at $s = 1.92$. In the slow modulation limit, where s is large, $\tilde{\delta}(\tilde{t})$ reduces to power law decay and no recurrence is found. In the fast modulation limit, where s approaches 1, reaction kinetic becomes single exponential and $\tilde{\delta}(\tilde{t})$ vanishes. It can also be observed in Figure 9 that the relation between the focal time and the echo time, $t_e = 2t_f$, remains valid and that the maximal echo occurs at $\lambda \approx \langle(\delta k)^2\rangle/\langle k\rangle$ as predicted by eq 35. The echo time, listed in Table 3, confirms the prediction of $t_e = 2/(\langle k\rangle + \gamma)$. The two-dimensional contour $\delta(t_1,t_2)$ (not included here) shows the same features as for the multiple-channel model. Thus, the conformational fluctuation rate in the diffusion model has a strong influence on the two-event echo signal in the same-time difference function. However, because of its single-channel nature in the inhomogeneous limit, the diffusion model predicts weaker echo signals than the multiple-channel model.

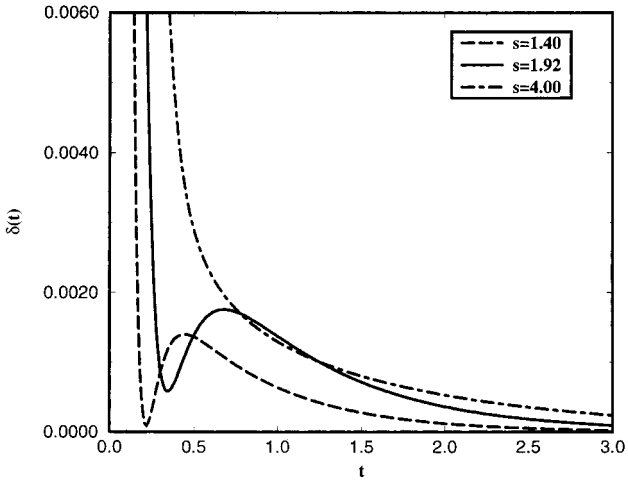

Figure 9. s dependence of the same-time difference function $\delta(t)$ in the continuous diffusion model. $s = \sqrt{1+4\kappa\theta/\lambda}$, reflects the competition between the time scales of the diffusion and the rate process. $\delta(t)$ is normalized by $\delta(0)$, and the time variable is scaled by $1/(\kappa\theta)$.

TABLE 3: Echo Time in the Diffusion Model with $\kappa_\theta = 1.0$[a]

λ	2.5	2.5	3.0	3.5	4.0
$t_{e,pred}$	0.667	0.571	0.500	0.444	0.400
$t_{e,meas}$	0.615	0.560	0.520	0.485	0.455
error	8.5%	2.0%	3.8%	8.5%	12%

[a] $t_{e,pred}$ is calculated by $t_{e,pred} = 2/(\langle k\rangle + \lambda)$, and $t_{e,meas}$ is obtained from the numerical calculation of $\tilde{\delta}(\tilde{t})$ in eq 51. The error is defined as $|t_{e,pred} - t_{e,meas}|/t_{e,meas} \times 100\%$.

VI. Stochastic Rate Model

The analysis of on−off sequences is usually based on specific kinetic schemes and assumed functional forms. Different versions of the discretized multiple-channel model include the two-channel two-state scheme, two-channel three-state scheme, and three-channel two-state scheme. In the continuous limit, a diffusion coordinate is introduced to modulate the rate constant: the exponential dependence was used to describe diffusion-controlled ligant binding and more recently enzymatic reactions,[28] the localized population sink was used for solvent-controlled electron transfer, and the quadratic dependence was used to describe stochastic gating.[31] To analyze and compare single-molecule quantities predicted by various reaction schemes in a unified framework, we adopt a general approach based on the stochastic rate model and the cumulant expansion.[46,47] In this model, environmental fluctuations introduce time-dependence in the rate constant, which is treated as a stochastic variable. Each realization of the time-dependent rate constant defines a rate process, and single molecular measurements can be obtained after taking the stochastic average of rate fluctuations. This approach is inspired by Kubo's stochastic lineshape theory because the rate constant in the rate model and the frequency in the Kubo's model are both treated as stochastic variable.[35] In principle, the stochastic properties of the rate are completely described by all of the multiple time cumulants. In practice, we truncate the cumulant expansion to second order in time variables, thus yielding a *Gaussian stochastic rate model*. The analysis of single-molecule quantities in the Gaussian approximation is similar to the study of spectral diffusion at cryogenic temperatures by Silbey and co-workers and Skinner and co-workers.[48,49] Then, various reaction schemes can be mapped to the Gaussian stochastic rate model characterized by average rate constants and rate correlation functions, and all single-molecule quantities can be evaluated accordingly.

A. Cumulant Expansion of the Stochastic Rate Model. The rate constant, modulated by slow environmental fluctuations,

can be treated as a stochastic variable. For the forward half-reaction

$$\text{on} \xrightarrow{k(\tau)} \text{off} \tag{52}$$

the survival probability distribution function is given by

$$P(t)= \langle \exp(-\int_0^t k(\tau)\, d\tau)\rangle \tag{53}$$

where $k(\tau)$ is the stochastic rate variable. Cumulant expansion of eq 53 leads to

$$P(t) = \exp\left[\sum_{n=1}^{\infty}\frac{(-1)^n}{n!}\int_0^t d\tau_1 \cdots \int_0^t d\tau_n\, \chi_n(\tau_1,...,\tau_n)\right] \tag{54}$$

where $\chi_n(\tau_1,...,\tau_n)$ is the nth order correlation function defined as

$$\begin{aligned}
\chi_1(t) &= \langle k(t)\rangle \\
\chi_2(t_1,t_2) &= \langle k(t_1)k(t_2)\rangle - \langle k(t_1)\rangle\langle k(t_2)\rangle \\
\chi_3(t_1,t_2,t_3) &= \langle k(t_1)k(t_2)k(t_3)\rangle - \langle k(t_1)\rangle\langle k(t_2)k(t_3)\rangle - \\
&\quad \langle k(t_2)\rangle\langle k(t_1)k(t_3)\rangle - \langle k(t_3)\rangle\langle k(t_1)k(t_2)\rangle + \\
&\quad 2\langle k(t_1)\rangle\langle k(t_2)\rangle\langle k(t_3)\rangle \\
&\quad ...
\end{aligned} \tag{55}$$

These cumulant functions contain all of the information necessary to describe the dynamics of modulated rate processes; thus, all of the single-molecule quantities can be expressed in cumulants with different weights. Some examples are given in Appendices B and C.

For a stationary Gaussian process, $\chi_k(t_1,...,t_k) = 0$ (for $k > 2$) and $\chi_2(t_1,t_2) = \chi(t_1 - t_2)$, the survival probability is simplified to

$$P(t) = \exp[-\langle k\rangle t + M(t)] \tag{56}$$

where $M(t) = \int_0^t (t - \tau)\chi(\tau)\, d\tau$ is the second-order cumulant. The distribution function of single on-time events is related to the survival probability by

$$F(t) = -\frac{dP(t)}{dt} \tag{57}$$

which, for the stationary Gaussian case, becomes

$$F(t) = (\langle k\rangle - \int_0^t \chi(\tau)\, d\tau)\exp[-\langle k\rangle t + M(t)] \tag{58}$$

Because the single-event distribution function is always finite, $\langle k\rangle \geq \int_0^t (1 - \tau/t)\chi(\tau)\, d\tau$ has to be satisfied at any time t. Especially, when t approaches infinity, $\langle k\rangle \geq \int_0^\infty \chi(\tau)\, d\tau$, i.e., there exists a finite time scale for conformational fluctuations. Given the finite time scale for conformational fluctuations, τ_c, the condition for the second-order cumulant expansion can be established as $\langle k\rangle \geq \chi(0)\tau_c$, implying a small variance of reaction rates and a short correlation time for conformational fluctuations.

The stochastic rate model is flexible in describing single-molecule measurements. With a proper choice of $\chi(t)$, the model can reproduce power-law and other nonexponential time dependence. The second cumulant expansion of the model, however, is only accurate for describing Gaussian processes. The deviation of real measurements from the second cumulant expansion is an indication of the non-Gaussian behavior.

B. Two-Event Echoes in the Gaussian Approximation. To simplify our calculations, we consider symmetric reactions with $k_f(t) = k_b(t) = k(t)$. In this case, the single-event and two-event distribution functions can be expressed as

$$f(t) = \frac{\langle k(t)\exp[-\int_0^t k(\tau)\, d\tau]k(0)\rangle}{\langle k\rangle} \tag{59a}$$

$$f(t_1,t_2) = \frac{\langle k(t_1+t_2)\exp[-\int_{t_1}^{t_1+t_2} k(\tau)\, d\tau]k(t_1)\exp[-\int_0^{t_1} k(\tau)\, d\tau]k(0)\rangle}{\langle k\rangle} \tag{59b}$$

For further simplification, we truncate the cumulant expansion to second order, giving

$$f(t) = \frac{[\langle k\rangle - L(t)]^2 + \chi(t)}{\langle k\rangle}\exp[-\langle k\rangle t + M(t)] \tag{60a}$$

$$\begin{aligned}
f(t_1,t_2) = \Big\{ &\langle k\rangle^2 - \langle k\rangle[2L(t_1+t_2) + L(t_1) + L(t_2)] + \chi(t_1) + \\
&\chi(t_2) + \chi(t_1+t_2) + 2L(t_1+t_2)[L(t_1) + I(t_2)] + L(t_1 + \\
&L_2)^2 - \frac{1}{\langle k\rangle}[\chi(t_1)L(t_1+t_2) + \chi(t_2)L(t_1+t_2) + \\
&\chi(t_1+t_2)L(t_1) + \chi(t_1+t_2)L(t_2) + L(t_1+t_2)L(t_1) + \\
&L(t_1+t_2)L(t_2)]\Big\}\exp[-\langle k\rangle(t_1+t_2) + M(t_1+t_2)]
\end{aligned} \tag{60b}$$

where $L(t) = \dot{M}(t) = \int_0^t \chi(\tau)\, d\tau$. The detailed derivation of eqs 60a and 60b can be found in Appendix B. Other related single-molecule quantities are defined in Appendix C.

In the short time limit, when $L(t) \ll \chi(t)/\langle k\rangle$, we have

$$\frac{f(t_1,t_2) - f(t_1)f(t_2)}{f(t_1)f(t_2)} \approx \frac{\chi(t_1+t_2) - \dfrac{\chi(t_1)\chi(t_2)}{\langle k\rangle^2}}{\left(\langle k\rangle + \dfrac{\chi(t_1)}{\langle k\rangle}\right)\left(\langle k\rangle + \dfrac{\chi(t_2)}{\langle k\rangle}\right)} \overset{t\to 0}{\approx} \frac{\chi(t_1+t_2)}{\langle k\rangle^2} \tag{61}$$

which indicates that $\chi(t)$ is a direct measure of memory effects in the initial decay regime.

The focal time and the echo time in the same-time difference function can be derived from the Taylor expansion of eqs 60a and 60b. We assume the exponential decay form of $\chi(t) = \chi(0)e^{-2\gamma t}$ for simplicity and the small variance condition of $\chi(0) \ll \langle k\rangle^2$, i.e., $k_d \ll k_s$, so that $L(t) = \chi(0)(1 - e^{-2\gamma t})/(2\gamma)$, $M(t) = \chi(0)(e^{-2\gamma t} - 1 + 2\gamma t)/(4\gamma^2)$. Then, to first order in the small parameter $\chi(0)/\langle k\rangle^2$, we have

$$\begin{aligned}
f(t) \approx \langle k\rangle\Big\{1 + \frac{\chi(0)}{\langle k\rangle^2}\Big[&e^{-2\gamma t} - \frac{\langle k\rangle}{\gamma}(1 - e^{-2\gamma t}) + \\
&\frac{\langle k\rangle^2}{4\gamma^2}(e^{-2\gamma t} + 2\gamma t - 1)\Big]\Big\}\exp(-\langle k\rangle t)
\end{aligned} \tag{62a}$$

$$\begin{aligned}
f(t,t) \approx \langle k\rangle^2\Big\{1 - \frac{\chi(0)}{\langle k\rangle^2}\Big[&e^{-4\gamma t} + 2e^{-2\gamma t} + \frac{\langle k\rangle}{\gamma}(e^{-4\gamma t} + \\
&e^{-2\gamma t} - 2) + \frac{\langle k\rangle^2}{4\gamma^2}(e^{-4\gamma t} + 4\gamma t - 1)\Big]\Big\}\exp(-2\langle k\rangle t)
\end{aligned} \tag{62b}$$

and the same-time difference function

$$\delta(t) \approx \chi(0)\left(\frac{\langle k\rangle + 2\gamma - \langle k\rangle e^{2\gamma t}}{2\gamma}\right)^2 \exp(-2\langle k\rangle t) \quad (63)$$

The minimum of $\delta(t)$ can be found at

$$t_f = \frac{1}{2\gamma}\ln\left[\frac{\langle k\rangle + 2\gamma}{\langle k\rangle}\right] \approx \frac{1}{\langle k\rangle + \gamma} \quad (64)$$

and the maximum at

$$t_e = \frac{1}{\gamma}\ln\left[\frac{\langle k\rangle + 2\gamma}{\langle k\rangle}\right] \approx \frac{2}{\langle k\rangle + \gamma} \quad (65)$$

The amplitude of the echo proportional to the variance of the rate constant, $\delta(t_e) \propto \chi(0)$. Thus, we obtain the same expressions for t_e and t_f as those derived for the two-channel model in section III. In Table 4, the echo time predicted from eq 60b, $t_{e,pred}$, is compared with the echo time calculated from the same-time distribution function, $t_{e,meas}$. Good agreement is found over a wide range of modulation rates γ between these two sets of echo times.

In Figure 10, the same-time difference function $\delta(t)$ calculated from eqs 60a and 60b is plotted for $k_s = \langle k\rangle = 3.0$ and $\gamma = 0.5$. For several values of $\chi(0) = k_d^2 = \langle \delta k^2\rangle$, the focal time and the echo time remain constant, but the amplitude of the echo increases proportionally with $\chi(0)$. In Figure 11, the echo time is shown to be twice the focal time and decreases with the modulation rate γ according $t_e = 2t_f = 2/(\langle k\rangle + \gamma)$. The maximal echo is found around $\gamma = \chi(0)/\langle k\rangle$. These features are consistent with our observations in the multiple-channel kinetic model.

C. Mapping to the Gaussian Stochastic Rate Model. We now map the discrete two-channel model to the Gaussian stochastic rate model. For simplicity, we consider a two-channel model with symmetric half-reactions, $\mathbf{K}_a = \mathbf{K}_b$, and with equal conformational states, $\gamma = \gamma'$. In this model, the survival probability function is $P(t) = [(\Delta + \gamma)e^{-Z_- t} + (\Delta - \gamma)e^{-Z_+ t}]/(2\Delta)$.[27] Matching the survival probability function with eq 56, we have, in the second cumulant approximation scheme, $\langle k\rangle = k_s$ and

$$\chi(t) = \frac{\Delta^2 k_d^{\,2}}{[\gamma \sinh(\Delta t) + \Delta \cosh(\Delta t)]^2} \quad (66)$$

which gives the variance $\chi(0) = k_d^2$ and the long-time correlation $\chi(t) \propto \exp(-2\Delta t)$. Figure 12 is a two-dimensional plot of $\delta(t_1,t_2)$ for the stochastic Gaussian model corresponding to a two-channel model with $k_1 = 2$, $k_2 = 4$, and $\gamma = 0.5$. In comparison with Figure 13, the stochastic Gaussian model reproduces all of the essential features of the difference function for the corresponding two-channel model. To be quantitative, the distribution functions of single events in Figure 13 agree very well by matching the survival probability. The same-time distribution functions calculated from the two models are compared in Figure 14, where the stochastic rate model is shown to give reasonable approximations to the position of the echo, the amplitude of the echo, and the shape of the same-time difference function. The slight deviations are believed to be the approximate nature of the second-order cumulant expansion, i.e., non-Gaussian effects.

VII. Summary

The aim of this paper is to establish a quantitative relation between the two-event echo and conformational fluctuations. The primary findings of our analysis can be summarized as follows:

TABLE 4: Echo Time in the Stochastic Rate Model with $\langle k\rangle = 3.0$ and $\chi(0) = 0.25$[a]

γ	0	0.5	1.0	1.5	2.0	2.5
$t_{e,pred}$	0.667	0.571	0.500	0.444	0.400	0.364
$t_{e,meas}$	0.665	0.575	0.515	0.465	0.425	0.395
error	0.3%	0.7%	2.9%	4.5%	5.9%	7.8%

[a] $t_{e,pred}$ is calculated with $t_{e,pred} = 2/(\langle k\rangle + \gamma)$, and $t_{e,meas}$ is obtained from numerical calculation of the stochastic rate model with $\chi(t) = \chi(0)^{-2\gamma t}$. The error is defined as $|t_{e,pred} - t_{e,meas}|/t_{e,meas} \times 100\%$.

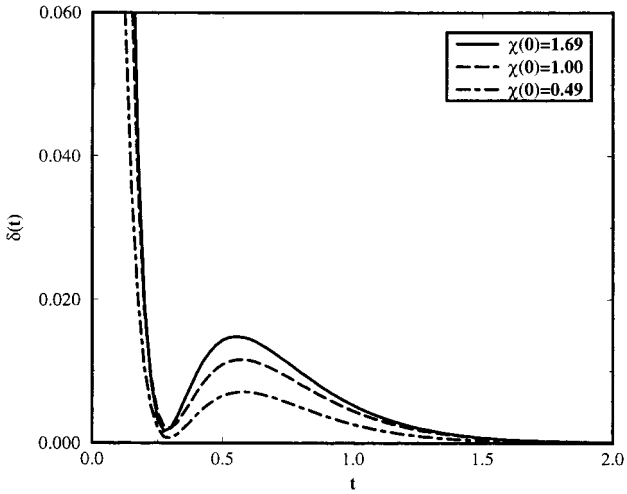

Figure 10. Two-event echo in the stochastic rate model with $\langle k\rangle = 3.0$, $\gamma = 0.5$, and $\chi(t) = \chi(0)e^{-2\gamma t}$. The echo time $t_e \approx 2/(\langle k\rangle + \gamma)$ is approximately fixed when varying $\chi(0)$, and the echo increases with $\chi(0)$.

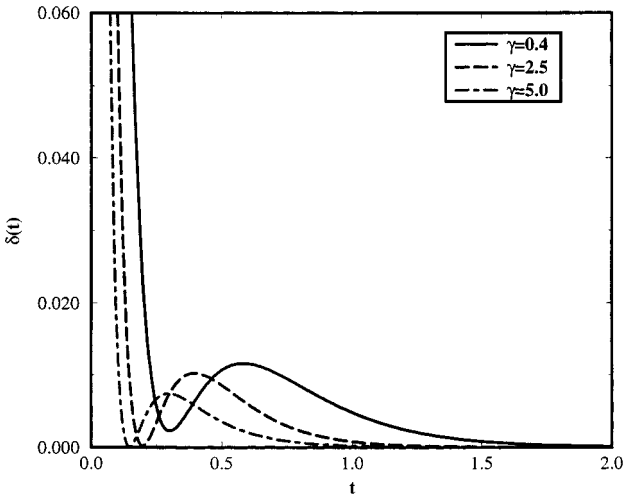

Figure 11. Two-event echo in the stochastic rate model with $\langle k\rangle = 3.0$, $\chi(0) = 1.0$, and $\chi(t) = \chi(0)e^{-2\gamma t}$. The echo time $t_e \approx 2/(\langle k\rangle + \gamma)$ decrease as γ increases. The maximum amplitude of the echo is flat within an interval of γ. The position of the maximal echo is approximately the medium of this interval, $\gamma \approx 0.4$.

1. The *N*-channel kinetic scheme provides a generic model for understanding the influence of conformational fluctuations on reaction dynamics. On the basis of this model, ensemble-averaged measurements can be formulated as a long-time average along single-molecule trajectories. As a result, phenomenological chemical kinetics is shown to be an inhomogeneous average of reaction rate constants and thus does not contain any information about dynamic disorder. It is also shown that the fluctuation−dissipation relation is obeyed on the single-molecule level only if the initial nonequilibrium disturbance is prepared according to conformational equilibrium. This condi-

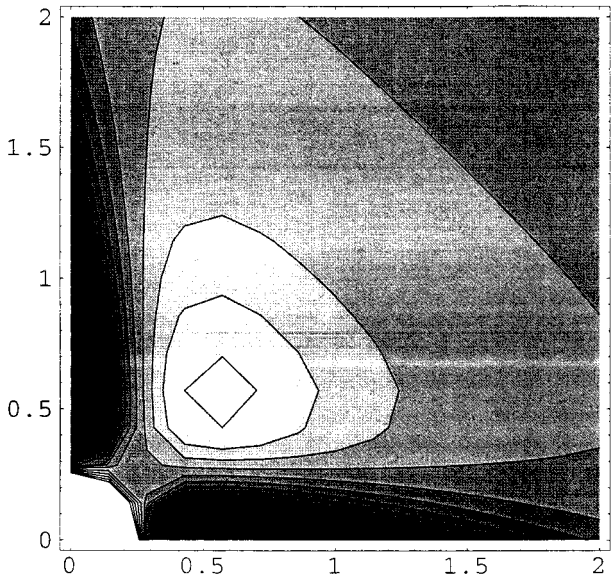

Figure 12. Two-dimensional contour plot of the joint distribution function of two events $\delta(t_1,t_2) = f(t_1,t_2) - f(t_1)f(t_2)$ in the stochastic rate model with $k_1 = 2$, $k_2 = 4$, and $\gamma = \gamma_1 = \gamma_2 = 0.5$. $f(t)$ and $f(t_1,t_2)$ are calculated by eqs 60a and 60b, respectively, with $\chi(t)$ in eq 66 obtained from matching the survival probability.

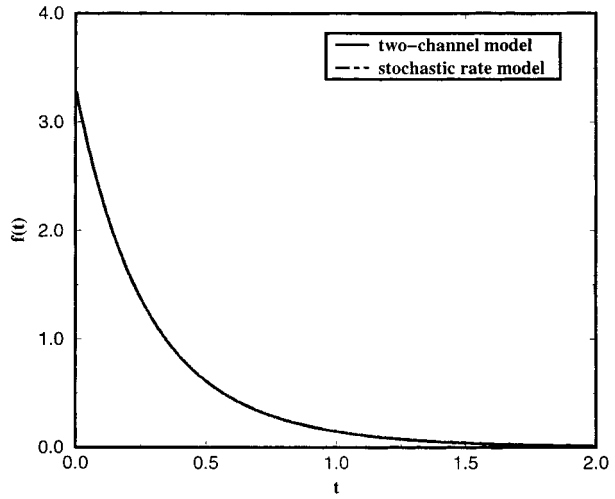

Figure 13. Comparison of the single-event distribution functions in the two-channel model and in the corresponding stochastic rate model with $k_1 = 2$, $k_2 = 4$, and $\gamma = 0.5$. The single-event distribution function $f(t)$ in stochastic rate model is calculated by eq 60a with $\chi(t)$ given in eq 66.

tion imposes a difficult condition on the use of ensemble-averaged measurements to probe conformational fluctuations. In addition, a more stringent detailed balance condition can be established to exclude the possibility of microscopic current between different conformational channels.

2. Calculations of four different models (the two-channel kinetic model, the three-channel kinetic model, the diffusion reaction model, and the stochastic rate model) confirm the universal features of the two-event joint distribution function and its quantitative relationship to conformational dynamics. In the two-dimensional plane of $\delta(t_1,t_2)$, there is a local minimum at the focal time, t_f, and a local maximum at the echo time, t_e, along the diagonal cross-section $\delta(t,t)$ and there is a minimum at the echo time along both the t_1 axis and the t_2 axis. The echo time is twice the focal time, $t_e = 2t_f$, and can be approximated, within 10% error, by $t_e = 2/(\langle k\rangle + \langle\gamma\rangle)$. This approximate relation is independent of the backward reaction, the distribution

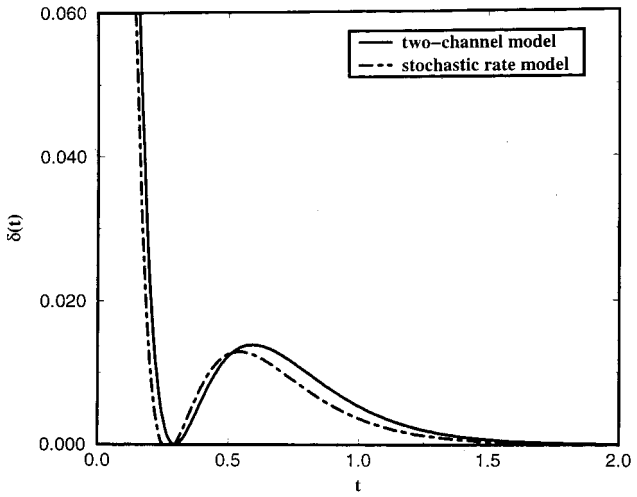

Figure 14. Comparison of the same-time difference function $\delta(t)$ in the two-channel model and in the corresponding stochastic rate model with $k_1 = 2$, $k_2 = 4$, and $\gamma = 0.5$. The stochastic rate model gives good approximations to the echo time, the echo height, and the shape of $\delta(t)$.

of the reaction rate constant, and other variables, thus resulting in a direct estimation of the average relaxation rate of conformational fluctuations, for a given ensemble-averaged reaction rate constant.

3. The correlation between the amplitude of the echo and the distribution of reaction rate constants provides useful information about conformational landscapes. The amplitude of the echo is shown to be proportional to the variance of the reaction rate constant, $\delta(t_e) \propto \langle\delta k^2\rangle$. For a given set of reaction rate constants, the maximum echo occurs at approximately $\gamma \approx \langle(\delta k)^2\rangle/\langle k\rangle$, which is proportional to the variance of the reaction rate constant. In the slow modulation limit, the existence of the two-event echo can be related to the individuality and distinctiveness of conformational landscapes. The maximum echo occurs when the difference between rate constants associated with different conformational channels is maximized, whereas the difference between reactive fluxes is minimized.

4. The stochastic rate model provides a complete and unified description of the stochastic nature of the fluctuating rate constant. Its second-order cumulant expansion, on the basis of the small variance assumption, leads to the Gaussian stochastic rate model that serves as a first-order model for analyzing single-molecule trajectories. Similar to Kubo's stochastic lineshape theory, the stochastic Gaussian model describes the fluctuating rate process with an average rate constant $k_s = \langle k\rangle$ and a rate correlation function $\chi(t) = \langle[k(t) - k_s][k(0) - k_s]\rangle$. The resulting formalism reproduces the recurrent behavior in the two-event joint distribution function. Through the mapping to the Gaussian stochastic rate model, various modulated reaction schemes can be compared and characterized in a unified framework.

These results provide a quantitative tool to interpret and analyze event-averaged single-molecule quantities. Though a single time scale for conformational fluctuations is assumed for the simplicity of calculations, applications of current analysis to power-law decay and other nonexponential relaxation processes can also be formulated. Furthermore, conformational relaxation is reflected not only in modulated reactions but also in other dynamic processes, including diffusion and quantum dissipation. Theoretical analysis of possible single-molecule

measurements of these processes is an interesting topic for future studies.[50−53]

Acknowledgment. The research is supported by the AT&T Research fund Award and the NSF Career Award (Che-0093210).

Appendix A: The Green's Function in the Diffusion Model

Equation 41 satisfies the Smoluchowski equation with a quadratic sink

$$\frac{\partial}{\partial t}G(x,y,t) = -\kappa x^2 G(x,y,t) + \lambda\theta\frac{\partial}{\partial x}\left(\frac{\partial}{\partial x}+\frac{x}{\theta}\right)G(x,y,t) \quad \text{(A1)}$$

with the initial condition

$$G(x,y,0) = \delta(x-y) \quad \text{(A2)}$$

Applying the transformation

$$G(x,y,t) = g(x,y,t)\mathrm{e}^{\alpha(x^2-y^2)} \quad \text{(A3)}$$

where $\alpha = (s-1)/(4\theta)$, $s = \sqrt{1+4\kappa\theta/\lambda}$, we find that $g(x,y,t)$ satisfies the Fokker−Planck equation for the Ornstein-Uhlenbeck process with a constant potential sink

$$\frac{\partial}{\partial t}g(x,y,t) = \left[\lambda s\frac{\partial}{\partial x}x + \lambda\theta\frac{\partial^2}{\partial x^2}\right]g(x,y,t) - \frac{\lambda}{2}(s-1)g(x,y,t) \quad \text{(A4)}$$

with the initial condition

$$g(x,y,t) = \delta(x-y) \quad \text{(A5)}$$

Further, we rewrite $g(x,y,t)$ as

$$g(x,y,t) = g_1(x,y,t)\mathrm{e}^{-\lambda/2(s-1)t} \quad \text{(A6)}$$

where $g_1(x,y,t)$ is the Green's function for the standard Ornstein-Ulenbeck process.

$$\frac{\partial P}{\partial t} = \gamma\frac{\partial}{\partial x}(xP) + D\frac{\partial^2 P}{\partial x^2} \quad \text{(A7)}$$

with $\gamma = \lambda s$ and $D = \lambda\theta$. The standard solution to eq A7 is given in ref 54 as

$$g_1(x,y,t) = \sqrt{\frac{\gamma}{2\pi D(1-\mathrm{e}^{-2\gamma t})}}\exp\left[-\frac{\gamma(x-y\mathrm{e}^{-\gamma t})^2}{2D(1-\mathrm{e}^{-2\gamma t})}\right] \quad \text{(A8)}$$

Therefore, the Green's function for the Ornstein-Uhlenbeck process in a constant potential sink is

$$g(x,y,t) = \mathrm{e}^{-\lambda(s-1)t/2}\left[\frac{s}{2\pi\theta(1-\mathrm{e}^{-2\lambda s t})}\right]^{1/2}\exp\left[-\frac{s(x-y\mathrm{e}^{-\lambda s t})^2}{2\theta(1-\mathrm{e}^{-2\lambda s t})}\right] \quad \text{(A9)}$$

which, after the transformation in eq A3, leads to $G(x,y,t)$ in eq 41. The same result was obtained by G. H. Weiss in ref 55. The equivalence can be confirmed by replacing D, β, and α in his derivation with $\lambda\theta$, $1/\theta$, and κ in our notation.

Appendix B: Single-Event and Two-Event Distribution Functions in the Gaussian Stochastic Rate Model

We first define a two-time survival probability function as

$$P(t_0,t_1) = \langle\exp[-\textstyle\int_{t_0}^{t_1}k(\tau)\,\mathrm{d}\tau]\rangle_s \quad \text{(B1)}$$

where the $\langle\cdots\rangle_s$ represents a stochastic average. Then, the single-event distribution function $f(t)$ defined in eq 59b can be related to $P(t_0,t_1)$ by

$$f(t) = -\frac{1}{\langle k\rangle}\frac{\partial^2 P(t_0,t_1)}{\partial t_0\,\partial t_1}\Big|_{t_0=0,t_1=t} = \frac{\langle k(t)\exp(-\int_0^t k(\tau)\,\mathrm{d}\tau)k(0)\rangle}{\langle k\rangle} \quad \text{(B2)}$$

The second cumulant expansion truncated at second order gives $P(t_0,t_1)$ explicitly as

$$P(t_0,t_1) = \exp[-\langle k\rangle(t_1-t_0) + M(t_1-t_0)] \quad \text{(B3)}$$

where $M(t) = \int_0^t(t-\tau)\chi(\tau)\,\mathrm{d}\tau$. Substitution of eq B3 into eq B2 leads to $f(t)$ in eq 60a. Similarly, a four-time survival probability function is defined as

$$P(t_0,t_1,t_1',t_2') = \langle\exp[-(\textstyle\int_{t_0}^{t_1}+\int_{t_1'}^{t_2'})k(\tau)\,\mathrm{d}\tau]\rangle_s \quad \text{(B4)}$$

The two-event distribution function $f(t_1,t_2)$ defined in eq 59b is related to $P(t_0,t_1,t_1',t_2')$ by

$$f(t_1,t_2) = \frac{1}{\langle k\rangle}\frac{\partial^3 P(t_0,t_1,t_1',t_2')}{\partial t_0\,\partial t_1\,\partial t_2'}\Big|_{t_0=0,t_1'=t_1,t_2'=t_1+t_2} = \frac{\langle k(t_1+t_2)\exp(-\int_{t_1}^{t_1+t_2}k(\tau)\,\mathrm{d}\tau)k(t_1)\exp(-\int_0^{t_1}k(\tau)\,\mathrm{d}\tau)k(0)\rangle}{\langle k\rangle} \quad \text{(B5)}$$

The four-time survival probability function $P(t_0,t_1,t_1',t_2')$ is obtained in the second cumulant approximation as

$$P(t_0,t_1,t_1',t_2') = \exp[-\langle k\rangle(t_1+t_2'-t_1'-t_0) + M(t_1-t_0) + M(t_2'-t_1') + M(t_2'-t_0) - M(t_1'-t_0) - M(t_2'-t_1) + M(t_1'-t_1)] \quad \text{(B6)}$$

which in combination with eq B5 leads to eq 60b.

Appendix C: Other Single-Molecule Quantities in the Gaussian Stochastic Model

In the forward half-reaction of the stochastic rate model, the normalized correlation function of two on-time events of durations t_1 and t_2 separated by time τ is expressed as

$$C_{\mathrm{on}}(t_1,\tau,t_2) = \frac{\langle\exp(-\int_0^{t_1}k_{\mathrm{f}}(t')\,\mathrm{d}t')\exp(-\int_{t_1}^{t_1+\tau+t_2}k_{\mathrm{f}}(t')\,\mathrm{d}t')\rangle}{\langle\exp(-\int_0^{t_1}k_{\mathrm{f}}(t')\,\mathrm{d}t')\rangle\langle\exp(-\int_{t_1}^{t_1+\tau+t_2}k_{\mathrm{f}}(t')\,\mathrm{d}t')\rangle} \quad \text{(C1)}$$

The second-order truncation of eq C1 leads to

$$C_{\mathrm{on}}(t_1,\tau,t_2) = \exp[M(t_1+t_2+\tau) + M(\tau) - M(t_1+\tau) - M(t_2+\tau)] \quad \text{(C2)}$$

where $M(t) = \int_0^t (t - \tau)\chi_{on}(\tau)\, d\tau$. In the small time limit, the above expression reduces

$$\lim_{t_1,t_2\to 0} \frac{C_{on}(t_1,\tau,t_2) - 1}{t_1 t_2} = \chi_{on}(\tau) \tag{C3}$$

which provides a direct measure of the rate correlation function $\chi_{on}(t)$.

Another function to illustrate memory effects is the on−off population correlation function

$$C(t) = \frac{\langle \delta\rho_{off}(t)\delta\rho_{on}(0)\rangle}{\langle \delta\rho_{off}(0)\delta\rho_{on}(0)\rangle} \tag{C4}$$

where $\rho_{on}(t)$ and $\rho_{off}(t)$ satisfy the master equation for the full reaction

$$\begin{pmatrix} \dot{\rho}_{on}(t) \\ \rho_{off}(t) \end{pmatrix} = \begin{pmatrix} -k_f(t) & k_b(t) \\ k_f(t) & -k_b(t) \end{pmatrix} \begin{pmatrix} \rho_{on}(t) \\ \rho_{off}(t) \end{pmatrix} \tag{C5}$$

Using the second cumulant expansion, the on−off population correlation function can be derived as

$$C(t) = \exp[-2\langle k\rangle t + 4M(t)] \tag{C6}$$

where the forward and the backward reactions are assumed to be equivalent.

References and Notes

(1) Berne, B. J. *Statistical Mechanics, Part B: Time-dependent Processes*; Plenum Press: New York, 1977.
(2) Cukier, R. I.; Deutch, J. M. *Phys. Rev.* **1969**, *177*, 240.
(3) Agmon, N.; Hopfield, J. J. *J. Chem. Phys.* **1983**, *79*, 2042.
(4) Straub, J. E.; Borkovec, M.; Berne, B. J. *J. Chem. Phys.* **1986**, *84*, 1788.
(5) Tang, H.; Jang, S.; Zhou, M.; Rice, S. A. *J. Chem. Phys.* **1994**, *101*, 8737.
(6) Zhou, M.; Rice, S. A. *Int. J. Quantum Chem.* **1996**, *58*, 593.
(7) Heller, E. J. *J. Chem. Phys.* **1995**, *99*, 2625.
(8) Pechukas, P.; Ankerhold, J. *J. Chem. Phys.* **1997**, *107*, 2444.
(9) Bache, T.; Moerner, W. E.; Orrit, M.; Wild, U. P. *Single-molecule optical detection, imaging and spectroscopy*; VCH Publishers: New York, 1996.
(10) Moerner, W. E.; Orrit, M. *Science* **1999**, *283*, 1670.
(11) Nie, S.; Zare, R. N. *Annu. Rev. Biophys. Biomol. Struct.* **1996**, *26*, 567.
(12) Ambrose, W. P.; Goodwin, P. M.; Martin, J. C.; Keller, R. A. *Science* **1994**, *265*, 364.
(13) Edman, L.; Mets, U.; Rigler, R. *Proc. Natl. Acad. Sci. U.S.A.* **1996**, *93*, 6710.
(14) Jia, Y.; Sytnik, A.; Li, L.; Vladimirov, S.; Cooperman, B. S.; Hochstrasser, R. M. *Proc. Natl. Acad. Sci. U.S.A.* **1997**, *94*, 7932.
(15) Lu, H. P.; Xun, L.; Xie, X. S. *Science* **1998**, *282*, 1877.
(16) Ha, T.; Ting, A. Y.; Liang, J.; Deniz, A. A.; Chemla, D. S.; Schultz, P. G.; Weiss, S. *Chem. Phys.* **1999**, *247*, 107.
(17) Baumann, C. G.; Bloomfield, V. A.; Smith, S. B.; Bustanmante, C.; Wang, M. D.; Block, S. M. *Biophys. J.* **2000**, *78*, 1965.
(18) Moerner, W. E. *Science* **1994**, *265*, 46.
(19) Skinner, J. L.; Moerner, W. E. *J. Phys. Chem.* **1996**, *100*, 13251.
(20) Reilly, P.; Skinner, J. L. *Phys. Rev. Lett.* **1993**, *71*, 4257.
(21) Brown, F. L. H.; Silbey, R. J. *J. Chem. Phys.* **1998**, *108*, 7434.
(22) Barkai, E.; Silbey, R. *Chem. Phys. Lett.* **1999**, *310*, 287.
(23) Xie, X. S.; Trautman, J. K. *Annu. Rev. Phys. Chem.* **1998**, *49*, 441.
(24) Geva, E.; Skinner, J. L. *Chem. Phys. Lett.* **1998**, *288*, 225.
(25) Berezhkovskii, A. M.; Szabo, A.; Weiss, G. H. *J. Chem. Phys.* **1999**, *110*, 9145.
(26) Schenter, G. K.; Lu, H. P.; Xie, X. S. *J. Phys. Chem. A* **1999**, *103*, 10499.
(27) Cao, J. *Chem. Phys. Lett.* **2000**, *327*, 38.
(28) Agmon, N. *J. Phys. Chem. B* **2000**, *104*, 7830.
(29) Frauenfelder, H.; Wolynes, P. G. *Science* **1985**, *229*, 337.
(30) Rector, K. D.; Engholm, J. R.; Rella, C. W.; Hill, J. R.; Dlott, D. D.; Fayer, M. D. *J. Chem. Phys.* **1999**, *103*, 2381.
(31) Wang, J.; Wolynes, P. *Phys. Rev. Lett.* **1995**, *74*, 4317.
(32) Onuchic, J. N.; Wang, J.; Wolynes, P. G. *Chem. Phys.* **1999**, *247*, 89.
(33) Chernyak, V.; Schuls, M.; Mukamel, S. *J. Chem. Phys.* **1999**, *111*, 7416.
(34) Weston, K.; Carson, P. J.; Metiu, H.; Buratto, S. K. *J. Chem. Phys.* **1998**, *109*, 7474.
(35) Kubo, R.; Toda, N.; Hashitsume, N. *Statistical Physics II*; Springer-Verlag: Berlin, Germany, 1985.
(36) Mukamel, S. *The Principles of Nonlinear Optical Spectroscopy*; Oxford University Press: New York, 1995.
(37) Northrup, S. H.; Hynes, J. T. *J. Chem. Phys.* **1980**, *73*, 2700.
(38) Grote, R. F.; Hynes, J. T. *J. Chem. Phys.* **1980**, *73*, 2715.
(39) Chandler, D. *Introduction to Modern Statistical Mechanics*; Oxford University Press: New York, 1987.
(40) Zwanzig, R. *J. Chem. Phys.* **1992**, *97*, 3587.
(41) Zusman, L. D. *Chem. Phys.* **1980**, *49*, 295.
(42) Sumi, H.; Marcus, R. A. *J. Chem. Phys.* **1986**, *84*, 4894.
(43) Hynes, J. T. *J. Phys. Chem.* **1986**, *90*, 3701.
(44) Yang, D. Y.; Cukier, R. I. *J. Chem. Phys.* **1989**, *91*, 281.
(45) Cao, J.; Jung, Y. *J. Chem. Phys.* **2000**, *112*, 4716.
(46) Kampen, N. G. van *Stochastic Processes in Physics and Chemistry*; North-Holland Physics: Amersterdam, The Netherlands, 1992.
(47) Ross, J.; Vlad, M. O. *Annu. Rev. Phys. Chem.* **1999**, *50*, 51.
(48) Suarez, A.; Silbey, R. *Chem. Phys. Lett.* **1994**, *218*, 445.
(49) Reilly, P. D.; Skinner, J. L. *J. Chem. Phys.* **1995**, *102*, 1540.
(50) Xu, X.; Yeung, E. S. *Science* **1997**, *275*, 1106.
(51) Schutz, G. J.; Schindler, H.; Schmidt, T. *Biophys. J.* **1997**, *73*, 1073.
(52) Cao, J. *Phys. Rev. E* **2001**, *63*, 041101.
(53) Cao, J. *J. Chem. Phys.* **2001**, *114*, 5138.
(54) Risken, H. *The Fokker−Planck Equation*; Springer-Verlag: New York, 1984.
(55) Weiss, G. H. *J. Chem. Phys.* **1984**, *80*.